Cumhuriyet Sci. J., 43(2) (2022) 333-341
DOI: https://doi.org/10.17776/csj.1037574

Cumhuriyet Science Journal

| csj.cumhuriyet.edu.tr | Founded: 2002 ISSN: 2587-2680 e-ISSN: 2587-246X Publisher: Sivas Cumhuriyet University

Altering Electrical Features of $LuFeO_3$ Compound Via Ir Doping into Fe Sites

Özgür Polat [1,2,a,*]

[1] CEITEC Brno University of Technology, Purkyňova 123, 612 00 Brno, Czech Republıc
[2] Institute of Physical Engineering, Brno University of Technology, Technická 2, 616 69 Brno, Czech Republıc
*Corresponding author

Research Article

History
Received: 16/12/2021
Accepted: 09/05/2022

ABSTRACT

Three ceramic compounds, $LuFeO_3$, $LuFe_{0.95}Ir_{0.05}O_3$, and $LuFe_{0.90}Ir_{0.10}O_3$, were synthesized via using solid-state reaction technique. Scanning electron microscopy (SEM) has been utilized to study surface morphology and the porous nature of the samples. The loss-tan(δ) of Ir substituted compounds are less than the undoped sample at frequencies > 10^5 Hz. The impedance study has revealed the Ir substituted samples have higher impedance values. Z" and M" vs frequency plots unveiled the existence of a non-Debye relaxation with short-range migration of carriers in the examined compounds. It has been shown 5 mol % Ir substituted specimen holds the maximum resistivity at 100^{0}C.

Keywords: Solid state reaction, The loss tangent, Complex impedance, Non-Debye relaxation, Resistivity.

[a] ozgurpolat7@gmail.com https://orcid.org/0000-0002-7410-1272

Introduction

It has been known that rare-earth orthoferrites having a formula of $RFeO_3$, here R refers to rare earth element, crystallize in distorted orthorhombic structure because of the spatial position of rare-earth compound and Fe^{3+} ions. It has been detailed that the optical, magnetic, and electrical characteristics of these materials can be altered by substitution into rare-earth and/or Fe compounds. Therefore, these materials have grabbed attention from the scientific community all over the globe [1,2]. Although these materials exhibit antiferromagnetic behavior having Neel temperature (T_N) = 630 K – 750 K, they can have weak ferromagnetic feature, which is owing to the tilted spin moment of Fe^{3+} ions. Furthermore, it has been shown these compounds display electric polarization [3] and hence, these materials are considered as multiferroic composites [4, 5]. In addition to magnetic features, it has been documented when the Fe sites are substituted with Os, Co, Ir dopants the optical features of rare-earth orthoferrites can be tuned [6-12]. $LuFeO_3$ (LFO), one of rare-earth compounds, illustrates significant distortion in the lattice due to Lu compound, which has ionic radius of 0.0861 for 3+ oxidation state, compared to the other earth compounds [13]. It is shown that LFO can have different crystalline structures depending upon fabrication method. For instance, it can hold hexagonal and orthorhombic structures [14,15]. LFO accommodates both magnetic and electrical features at the same time therefore it is considered as multiferroic material [16,17]. Due to low optical band gap of LFO, between ~ 2 eV for films and ~ 2.76 eV for ceramics [18,19], this compound has potential to be used in photocatalyst and solar cells [20]. Moreover, the magnetic and electrical properties of LFO are tuned by substitution of a wide range dopant elements into Lu and Fe sites such as Ni, Cr, Mn In, Sc, Bi and La [21-26]. The drives behind this investigation are as follows: 1) the first time Ir dopant, having 0.2 nm metallic radius and 0.0625 nm ionic radius for 4+ oxidation level, is exploited to scrutinize a) loss-tan(δ) versus frequency that quantifies how electromagnetic energy dissipates in the material, b) impedance versus frequency that i) inspects the influence of grains and grain boundaries on transport characteristics, ii) unveils the electrical response of various segments and the dynamic performance of confined and movable carriers in the bulk and interfacial areas, c) resistivity as function of frequency and temperature. Furthermore, Ir has been selected because it can have oxidation states from +1 to +9. As a result, its ionic radius varies depening on oxidation level. Such variations in both ionic radius and oxidation states influence optical, electrical, and magnetic properities of parent compound [27]. The previous investigtions documented Ir dopant, inducing both charge imbalance and distortion in the lattice structure, tunes both optical and electrical characteristics of $YbFeO_3$, which also belongs to rare-earth orthoferrite group [12, 13, 15].

In addition, a recent study has shown Ir substitution into Fe sites decreases the optical band gap of LFO from 2.19 eV to 2 eV [27]. It is known that the distortion taking place in the lattice structure influences characteristic features of materials. 2) Most of the investigations in the literature are related to the thin film of LFO with hexagonal structure. Hence, it is believed that this investigation helps to courge more examinations for the ceramic form LFO in the literature. The LFO and Ir doped LFO samples have been obtained via using solid-state technique. SEM was exploited to analyze the surface structure of the samples. The electrical properties of the investigated samples have scrutinized by Broadband Dielectric/Impedance Spectrometer.

Material and Method

Powder Preparation and Measurements

The powders and pellets preparations for the present study have been detailed in reference [28]. Surface morphology of the prepared pellets has been investigated by using Ultraplus Zeiss scanning electron microscopy (SEM). Broadband Dielectric/Impedance Spectrometer (Novocontrol Concept 50) has been exploited to examine the electrical properties of the undoped and Ir doped LFO compounds. The operating temperature for the electrical measurements has been gradually varied from -100°C to 100°C with 20°C temperature steps. The frequency was changed from 1 Hz to 10^7 Hz.

Results and Discussion

SEM Analyses

The previous investigation has examined the crystalline nature of the samples via using X-ray powder diffraction (XRD) [28]. It has been realized that the examined samples hold orthorhombic structure and Ir substitution leads to growth in the lattice volume. In addition, the XRD studies have revealed the creation of minor phases in the samples such as Lu_2O_3, $Fe_5Lu_3O_{12}$, $Fe_{21.16}O_{31.92}$, Fe_3O_4 and Ir_2Lu [28]. Furthermore, X-ray photoelectron spectroscopy (XPS) studies have laid down the valence states of Lu, Fe and Ir [28]. It has been unveiled that while Lu has 3+ state, Fe has mix of 2+ and 3+ valance states in the investigated samples. The oxidation state of Ir has been determined as 0 and 4+ in the Ir doped LFO samples. SEM examinations have shown the surface topography of the specimens and the obtained images are presented in Fig. 1. The initiation of agglomerations can be noticed in the samples. It should be bear in mind that such formation of agglomeration, caused by radical restructuring of particles at the initial phase of sintering, is common in the samples fabricated by solid-state reaction technique [6-12 17, 28]. The presence of voids can be also noticed in the images. Such void formations indicate that the samples have porous structure.

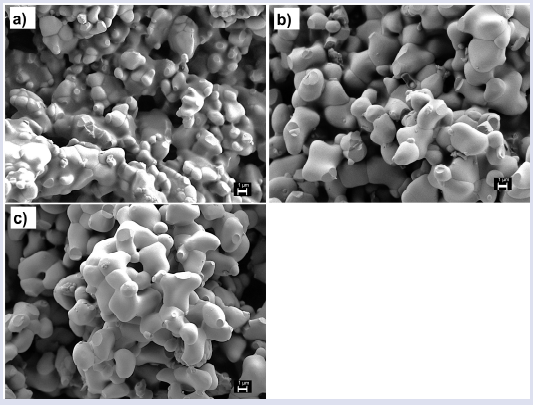

Figure 1. SEM images of studied samples a) LFO, b) 5% Ir and c) 10% Ir substituted LFO. Scale bar is 1 µm..

Electrical Measurements

The loss-tan(δ), tan(δ)=ε''/ε' where ε'' and ε' denote the imaginary and real part of dielectric function, respectively, indicates how electromagnetic energy dissipates in the material under the applied frequencies. Fig. 2 (semi-log scale) displays the loss-tan(δ) versus applied frequency, varying 1 Hz to 107 Hz, at temperature range of -100°C and 100 °C with ΔT = 20°C step for the investigated samples. Fig. 2 a) shows the loss-tan(δ) versus frequency spectra for undoped LFO sample. It appears that the loss-tan(δ) increases initially as the applied frequency raises and it makes a maximum peak (exhibiting relaxation process) then it decreases with further frequency at operating temperatures between -100°C and 0°C. While the maximum peak of loss-tan(δ) vs. frequency takes place around 10^2 Hz at -100 °C, it moves toward around 10^5 Hz at 0°C. When the operating temperature ≥ 20 °C, the company of two relaxation peaks, taking place at low and high frequencies, are noticeable. The first and second peaks appear around couple Hz and $2x10^5$ Hz at 20 °C, respectively. As the temperature advances, these peaks move to higher frequencies. Such as the first peak is noted ~ 10^3 Hz and second one is noticed ~ $5x10^6$ Hz at 100°C. Such movements of relaxation peaks underscore that the relaxation process is influenced by temperature [29, 30]. Fig. 2 b) and c) represent the loss-tan(δ) vs frequency for 5 mol and 10 mol % Ir doped LFO samples, respectively. It appears that the evolution of relaxation peaks is similar in both samples. Both samples have only one relaxation peak at all studied temperatures. The relaxation peak moves toward to higher frequencies as the temperature rises as observed in the undoped LFO sample. The comparison of the loss-tan(δ) vs frequency at 100°C is given for all the studied samples. It is seen the Ir doped samples exhibit lower loss-tan(δ) values than the undoped sample. Therefore, these materials with low loss-tan(δ) values might considered a potential candidate for the applications of new generation electronic device, which require to operate at high frequencies. It should be state here that loss-tan(δ) holds greater values at low frequencies that could be ascribed to 1) the presence of grain boundaries, which reduce/weaken the motion of charge carriers between ions and 2) the influence of interfacial loose. In addition, it is noticed that the loss-tan(δ) has higher values at higher temperatures at the same operating frequencies. Such behavior of loss-tan(δ) might be associated to the carrier exchange between Fe^{2+} and Fe^{3+} ions by resistive grain boundary.

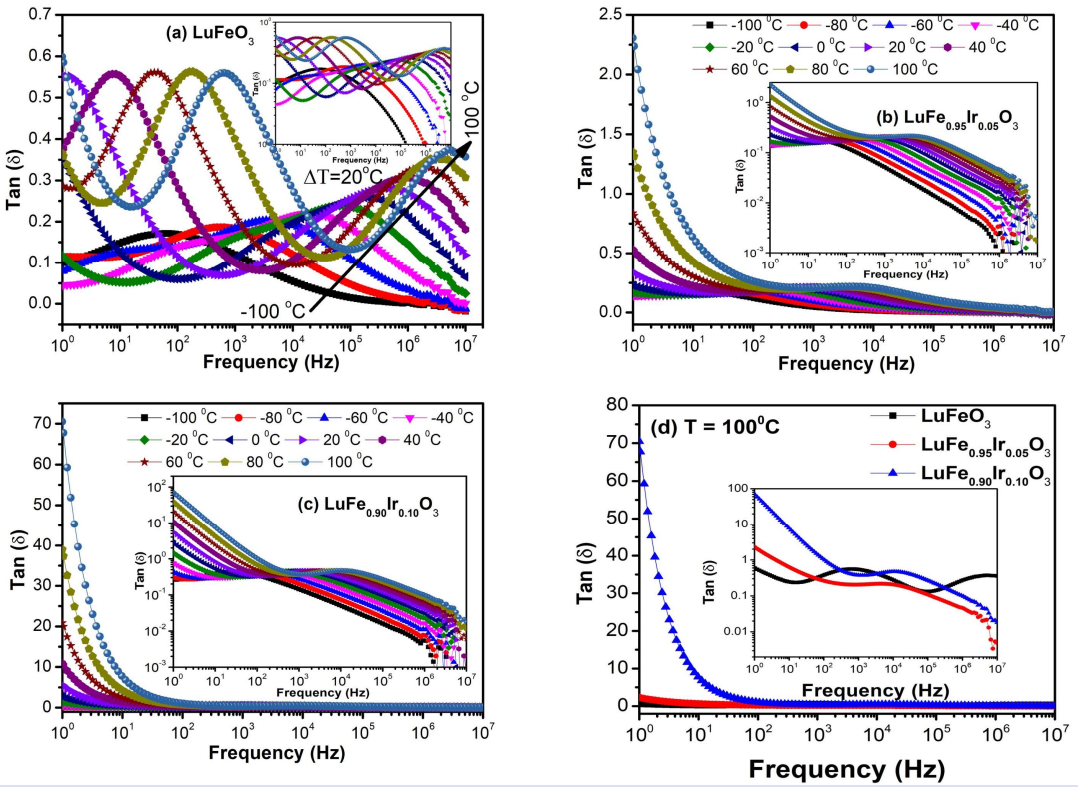

Figure 2. The tan (δ) for a) LFO, b) 5 mol % Ir and c) 10 mol % Ir doped LFO samples. d) represents the tan (δ) values of the studied samples at 100^{0}C. Inset figures are in log-log scale.

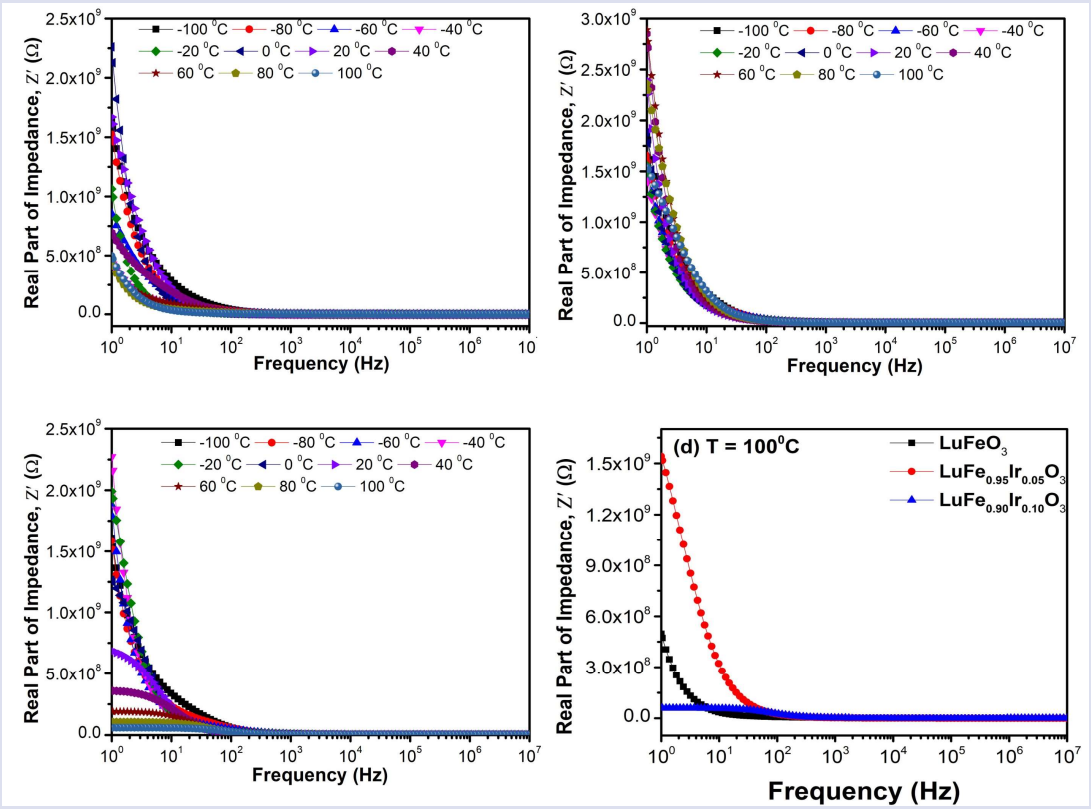

Figure 3. The tan (δ) for a) LFO, b) 5 mol % Ir and c) 10 mol % Ir doped LFO samples. d) represents the tan (δ) values of the studied samples at 100^{0}C. Inset figures are in log-log scale.

The impact of grain boundary, grain, and electrode on the electrical characterizations of materials have been investigated via impedance measurements [31]. The complex impedance, Z^*, is given by the following relation [32];

$$Z^* = Z' - jZ'' = \frac{1}{j2\pi f \varepsilon^* C_0} = \frac{\varepsilon'' - j\varepsilon'}{2\pi f C_0[(\varepsilon')^2 + (\varepsilon'')^2]} \quad (1)$$

here Z' denotes the real part, the imaginary part of impedance is shown by Z''. f, ε^*, and C_0 symbolize the frequency, complex dielectric function, and empty capacitance respectively. Fig. 3 (semi-log scale) exhibits the real part of impedance, Z', of the samples under scrutiny. It is noted the Z' values of studied samples reduce with increasing the frequency up to ~ 10 Hz and then the frequency free region is initiated at further applied frequencies due to reduction in energy barrier [33]. This plateau region is formed between 102 Hz- 107 Hz. It is also noted that frequency liberated area extends larger frequencies as the operating temperature surges. The comparison of Z' values of the inspected compounds is provided in Fig. 3 d) at 100°C. It is seen that 5 mol % Ir doped sample exhibits the maximum Z' values at 100°C until couple of hundred Hz then all the samples have the same Z' values at higher frequencies.

The imaginary part of impedance, Z", for the studied specimens is given in Fig. 4 in semi-log scale. It is noted the undoped sample has sharp decrease in Z" values at low frequencies (between 0 and ~ 30 Hz) and it forms plateau region, which is frequency independent area, at high frequencies, Fig. 4 a). Such behavior could be associated to the buildup of space charge carriers at high frequencies [34]. The undoped LFO sample does not exhibit relaxation peak at the investigated temperatures and frequencies in the instrument limit. Fig. 4 b) represents the Z" vs frequency for the 5 mol % Ir doped sample. Even though it exhibits similar frequency behavior at temperatures less than 80°C, the formation of relaxation peak, appearing around couple of Hz, can be noticed at 80°C and 100°C. Fig. 4 c) exhibits how Z" values vary with frequency and temperature in the case of 10 mol % Ir substitution. The initiation of relaxation peak becomes noticeable starting from -20°C at couple of Hz and the peak moves to ~ 10^2 Hz at 100°C. Fig. 4 d) compares the Z" values for the explored samples at 100°C. It appears that 5 mol % Ir doped has the largest Z" values close to 10^3 Hz. As the frequency is further advanced, the Z" values start to overlap.

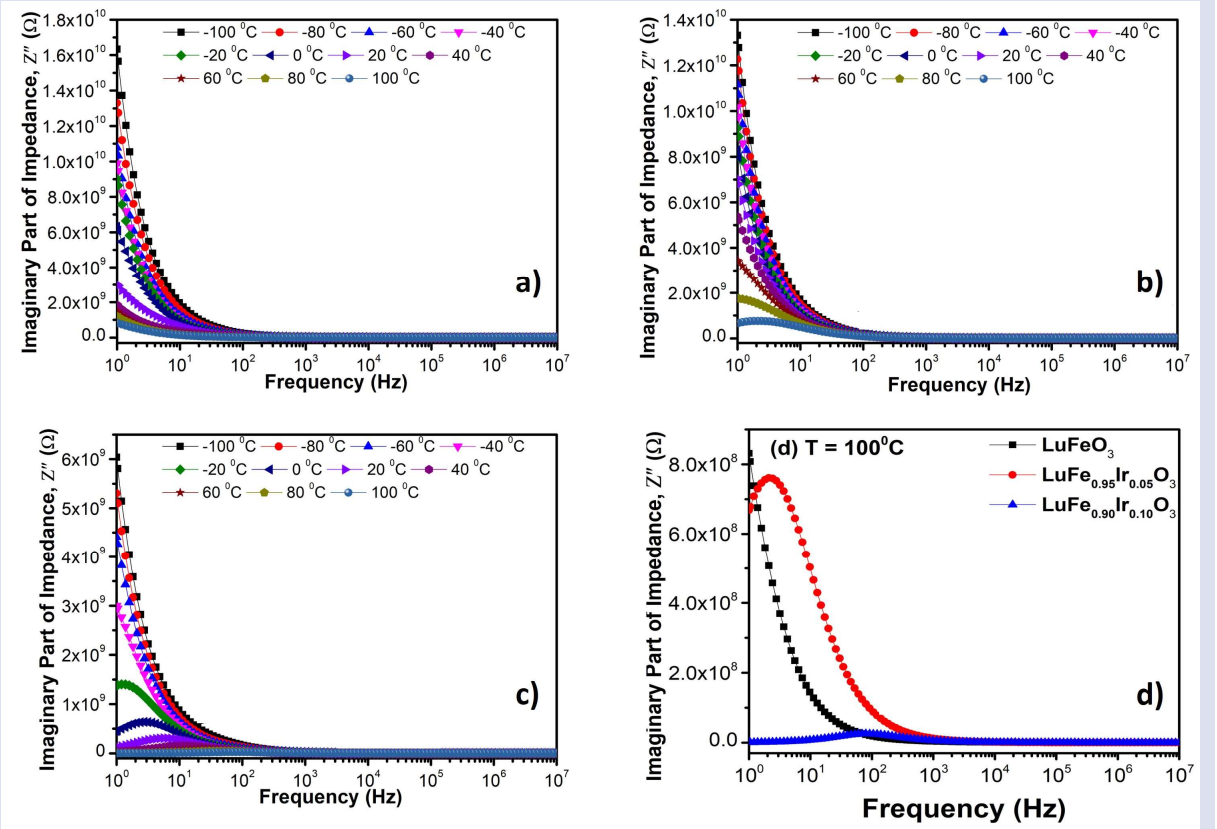

Figure 4. The imaginary part of impedance for a) LFO, b) 5 mol % Ir, c) 10 mol % Ir doped LFO composites. The comparison of imaginary part of impedances is given in d) at 100oC for all the samples.

Figure 5 exhibits Z″ and M″ vs. frequency spectra taken at two selected temperatures, -100^{0}C and 100^{0}C for LFO and Ir doped LFO samples. It is noted that Z″ vs. frequency plot does not exhibit the initiation of relaxation peak at both temperatures for the undoped LFO sample, Fig. 5 a), b). On the other hand, M″ vs. frequency spectra demonstrate the formation of relaxation peak at -100^{0}C and 100^{0}C for the same compound. The observed relaxation peaks are ascribed to grain at -100^{0}C and grain boundary at 100^{0}C, Fig. 5 a), b) respectively. Fig. 5 c) and d) represents the Z″ and M″ vs. frequency at -100^{0}C and 100^{0}C for the 5 mol % Ir substituted specimen, respectively. It is seen that Z″ vs. frequency plot does not have any relaxation peak at -100^{0}C, Fig. 5 c) while it reveals the creation of a peak at very low frequencies at 100^{0}C, Fig. 5 d). Nevertheless, M″ vs. frequency plot of the same sample has one peak, associated to the grain, at -100^{0}C, Fig. 5 c). When the operating temperature reaches 100^{0}C, the two peaks one at low frequency connected to the grain boundary and the second peak related to grain become eminent, Fig. 5 d).

In the case of 10 mol % Ir doped LFO sample, Z″ vs. frequency does not show any peak at -100^{0}C, Fig. 5 e). Yet, when the operating temperature becomes 100^{0}C, a relaxation peak is visible, which initiates around 200 Hz, Fig. 5 f). M″ vs. frequency spectra for the sample reveals the presence of one relaxation peak connected to the grain at -100^{0}C, Fig. 5 e). As temperature is further advanced to 100^{0}C, the existence of two relaxation peaks is noticed, Fig. 5 f). The first peak, which is attributed to the grain boundary, is visible around 10 Hz. The second peak is eminent around 5x10^4 Hz and this peak is related to the grains in the material. The joint plots of Z″ and M″ vs frequency are utilized to distinguish the type of relaxation process, a short range or long-range motion of carriers [34]. In the case of shorth-range movement, the peaks of Z″ and M″ vs frequency take place at dissimilar frequencies yet for the long-range migration of carriers the peaks overlap at the same frequencies [35]. In this investigation, it can be noted the peaks of Z″ and M″ *vs* frequency do not coincide at the same frequencies that underscores the existence of shorth-range migration of carriers. Furthermore, it is noted that there is a non-Debye relaxation happens in the studied samples.

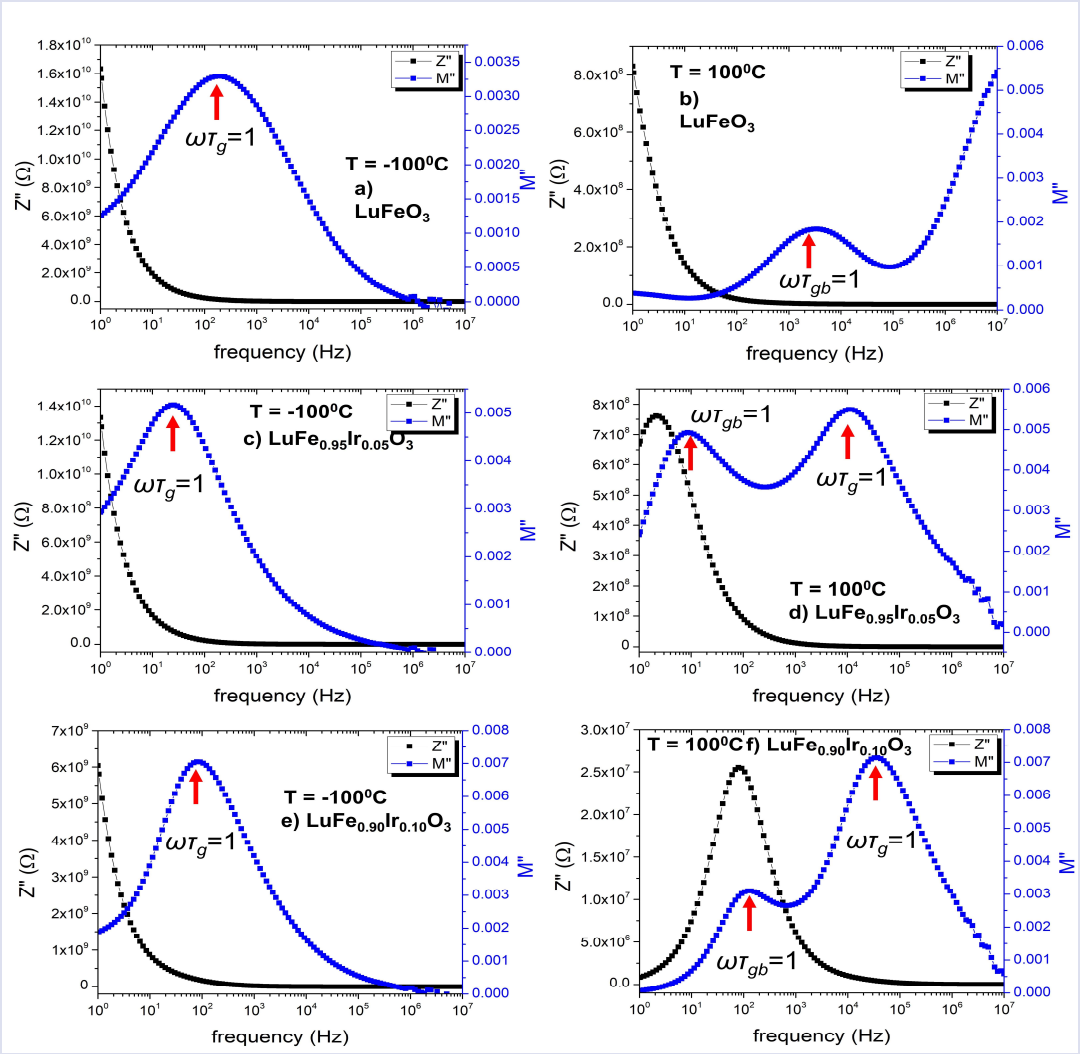

Figure 5. Z″ and M'' *vs.* frequency plots at (a) -100^{0}C and (b) 100^{0}C for LFO and (c) -100^{0}C and (d) 100^{0}C for 5 mol % Ir doped LFO sample, (e) -100^{0}C and (f) 100^{0}C for 10 mol % Ir substituted LFO compound.

Table 1. displays the temperature dependent relaxation time, capacitance and resistance of grain and grain boundary regions. These parameters have deducted by using $M''(\omega)$ *vs.* frequency spectra, shown in Fig. 5 in blue color, and following equations

$$M'' = \frac{C_0}{C}\left[\frac{\omega RC}{1+(\omega RC)^2}\right], \quad \tau = RC, \quad \omega = 2\pi f, \quad \omega\tau = 1 \tag{2}$$

here C_0, C, ω, R, τ and f represent empty capacitance of the sample, capacitance, angular frequency, resistance, relaxation time and linear frequency, respectively. It is noted that the obtained values diminish with raising the operating temperature. In addition, it is seen that the resistance value of the grain boundary is much higher than that of the grain. Such behavior can be associated to the charge transfer phenomenon in the grain and grain boundary areas. It is known that the carriers can migrate easier in the grain region compared to the grain boundary areas. That is why higher grain boundary resistance values are calculated. Furthermore, it is noticed that the resistance of both grain and grain boundary regions lowers with increasing the operating temperature, which is because of advancement in the carrier mobility pointing the semiconductor nature of the studied sample. The capacitance value of the grain and grain boundary drops with forwarding the temperature. This can be connected to the diminishing of charge accumulation near the grain boundary region. Because the thermal energy of carriers increases at high temperature and hence, they can move through the grain boundary region.

Table 1. The calculated resistance and other related parameters of undoped and Ir doped LFO compounds.

LuFeO3						
T (K)	τgb (s)	τg(s)	Cgb (F) x10^{-11}	Cg (F) x10^{-11}	Rgb (Ω)	Rg (Ω)
173		8.04x10-4		1.84		4.36x107
193		9.43x10-5		1.71		5.51x106
213		1.26x10-5		1.59		7.89x105
233		2.81x10-6		1.49		1.89x105
253		7.73x10-7		1.40		5.51x104
273		2.50x10-7		1.32		1.89x104
293	3.18x10-2	1.07x10-7	3.37	1.24	9.45x108	8.57x103
313	4.42x10-3	5.17x10-8	3.35	1.18	1.32x108	4.37x103
333	8.38x10-4	3.04x10-8	3.35	1.14		
353	1.88x10-4	1.41x10-8	3.33	1.12		
373	4.76x10-5		3.33			

$LuFe_{0.95}Ir_{0.05}O_3$						
T (K)	τgb (s)	τg(s)	Cgb (F) x10^{-11}	Cg (F) x10^{-11}	Rgb (Ω)	Rg (Ω)
173		7.96x10-3		2.41		3.31x108
193		2.70x10-3		2.39		1.13x108
213		1.21x10-3		2.37		5.10x107
233		5.81x10-4		2.33		2.50x107
253		2.94x10-4		2.29		1.28x107
273		1.54x10-4		2.26		6.79x106
293		8.73x10-5		2.25		3.89x106
313		4.96x10-5		2.25		2.21x106
333	9.37x10-2	3.18x10-5	2.67	2.25	3.50x109	1.41x106
353	3.98x10-2	2.03x10-5	2.62	2.25	1.52x109	9.02x105
373	1.77x10-2	1.30x10-5	2.52	2.25	7.02x108	5.78x105

$LuFe_{0.90}Ir_{0.10}O_3$						
T (K)	τgb (s)	τg(s)	Cgb (F) x10^{-11}	Cg (F) x10^{-11}	Rgb (Ω)	Rg (Ω)
173		2.27x10-3		1.42		1.60x108
193		8.17x10-4		1.42		5.74x107
213		3.51x10-4		1.42		2.47x107
233		1.67x10-4		1.41		1.18x107
253	7.96x10-2	8.78x10-5	3.76	1.41	2.12x109	6.24x106
273	3.54x10-2	4.59x10-5	3.73	1.41	9.48x108	3.27x106
293	1.59x10-2	2.66x10-5	3.68	1.41	4.33x108	1.89x106
313	7.96x10-3	1.54x10-5	3.58	1.41	2.22x108	1.09x106
333	3.98x10-3	9.85x10-6	3.48	1.41	1.14x108	7.00x105
353	2.21x10-3	6.61x10-6	3.33	1.41	6.63x107	4.70x105
373	1.16x10-3	4.47x10-6	3.25	1.41	3.58x107	3.18x105

The resistivity of the studied samples is given semi-log scale in Fig. 6 and inset images are provided in log-log scale. It is seen that the resistivity decreases as the applied frequency increases and resistivity values at different temperatures overlaps. Furthermore, it is noticed that the undoped and 5 mol % Ir doped samples do not show the formation of dc resistivity, Fig. 6 a) and b), respectively. On the other hand, the existence of dc resistivity becomes visible at temperature T ≥ 0°C at ~ 5 of Hz and it extends up to 10^2 Hz at 100°C, Fig. 6 c). The dc region is chased by ac resistivity, which decreases sharply with the applied frequency. Such decrement in resistivity with the frequency is associated to the exchanging of carriers between Fe^{2+} and Fe^{3+} ion sites [36]. Fig. 6 d) shows the comparison of the resistivities of examined samples at 100°C.

It is noted that 5 mol % sample has the highest resistivity. Such high resistivity of Ir substituted samples might be connected to lattice distortion created due to the Ir doping. The XPS analyses have unveiled that Ir has metallic and 4+ valence states in LFO structure. It needs to be cited that the radius of metallic Ir, which is 0.2 nm, is much larger than that of Fe^{2+} (0.078 nm) and Fe^{3+} (0.0645 nm) ions. Apparently, the lattice distortion is inevitable in LFO structure. Such lattice distortion can act carrier trap center and increase the resistivity of parent LFO compound [37]. A recent investigation about Os doping into Fe sites in LFO structure has also demonstrated similar trend [38]. Furthermore, it is known that conductivity or resistivity of rare-earth compounds is significantly influenced by carrier transfer between Fe^{2+} and Fe^{3+} ions in the system [36].

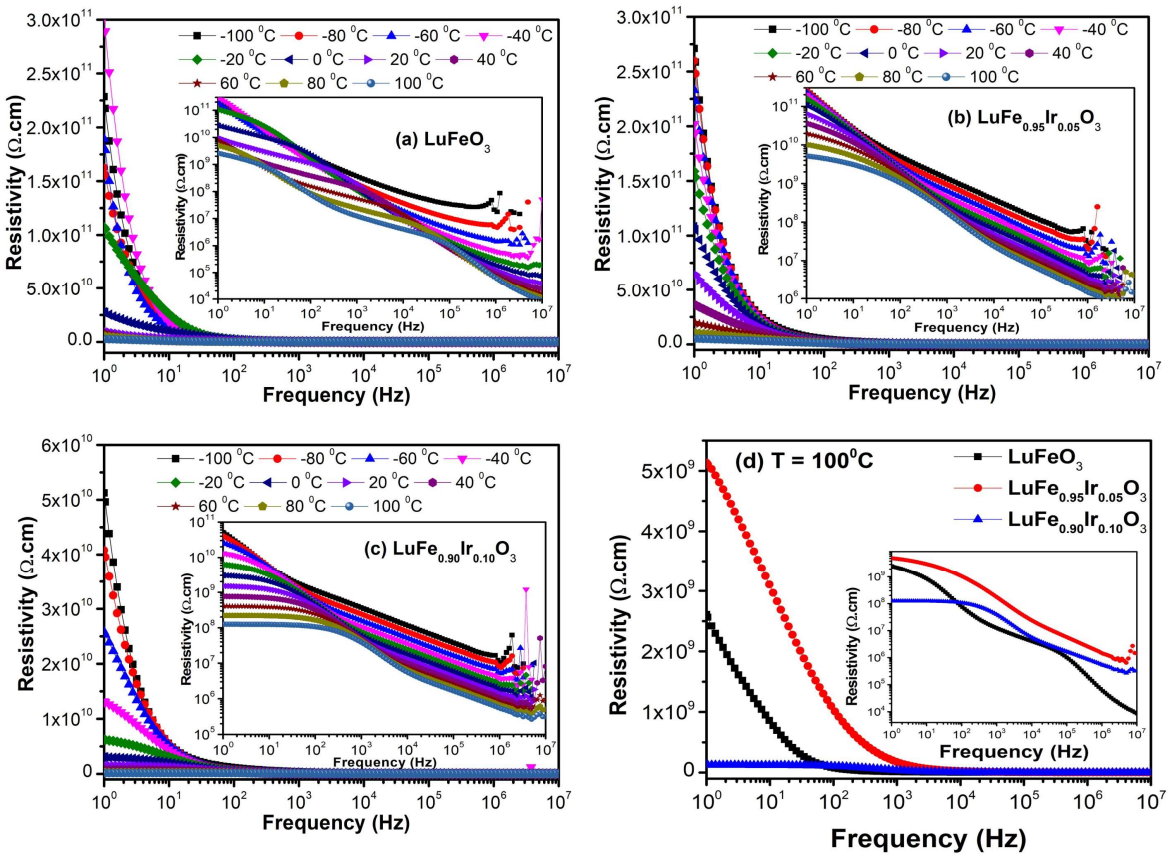

Figure 6. Resistivity of a) LFO, b) 5 mol %, c) 10 mol % Ir substituted LFO. d) Compares the resistivities at 100 °C. The inset images represent the log-log scale resistivity versus frequency.

Conclusions

The porous nature of the LFO and Ir substituted LFO ceramics were revealed by SEM analyses. It has been shown that Ir doped samples have lower loss- tan(δ) values at high frequency and temperature than LFO sample. Impedance study has demonstrated that at low frequencies the 5 mol % Ir substituted sample has the highest impedance values at 100 °C. Z″ and M″ *vs* frequency plots revealed that the presence of a non-Debye relaxation with short-range movement of carriers in the investigated samples. The resistivity studies have underlined that Ir doped sample possess the highest resistivity than the undoped LFO. The augmentation in the resistance could be connected to the lattice distortion and reduction in the ratio of Fe^{2+} ions, which is known that

conductivity of rare-earth compounds is significantly influenced by carrier transfer/hopping between Fe^{2+} and Fe^{3+} ions in the system. Recently, LFO has seized attention from scientific community because of its electrical, magnetic, and optical features. Therefore, the present study has detailed that the electrical, optical, and magnetic characteristics of LFO can be adjusted with Ir substitution. This study could pave the way for doping other transition elements into not only Fe but also Lu sites in LFO structure.

Acknowledgment

This work was supported by The Scientific and Technological Research Council of Turkey (TUBITAK) through Grant No: 116F025. The author would like to thank Prof. Dr. Abdulmecit Turut, Prof. Dr. Mujdat Caglar, Assoc. Prof. Mustafa Coskun, and Assoc. Prof. Zehra Durmus for their valuable comments.

Conflicts of interest

The authors state that did not have conflict of interests.

References

[1] Luo S.J., Li S.Z., Zhang N., Wei T., Dong X.W., Wang K.F., Liu J.M., Preparation of epitaxial $DyFeO_3$ thin films and magnetodielectric coupling, *Thin Solid Films,* 519 (2010) 240.

[2] Pomiro F., Sanchez R.D., Cuello G., Maignan A., Martin C., Carbonio R. E., Spin reorientation, magnetization reversal, and negative thermal expansion observed in $RFe_{0.5}Cr_{0.5}O_3$ perovskites (R=Lu,Yb,Tm), *Phys. Rev. B*., 94 (2016) 134402.

[3] Mandal P., Bhadram V.S., Sundarayya Y., Narayana C., Sundaresan A., Rao C. N. R., Spin-reorientation, ferroelectricity, and magnetodielectric effect in $YFe_{1-x}Mn_xO_3$ ($00.1 \le x \le 0.40$), *Phys Rev. Lett.,* 107(13) (2011) 137202.

[4] Yokota H., Nozue T., Nakamura S., Hojo H., Fukunaga M., Janolin P.-E., Kiat J.-M., Fuwa A., Ferroelectricity and weak ferromagnetism of hexagonal $ErFeO_3$ thin films, *Phys. Rev. B.*, 92(5) (2015) 054101.

[5] Song Y.-Q., Zhou W.-P., Fang Y., Yang Y.-T., Wang L.-Y., Wang D.-H., Du Y.-W., Multiferroic properties in terbium orthoferrite, *Chin. Phys. B.,* 23 (2014) 077505.

[6] Polat O., Coskun M., Coskun F. M., Kurt B. Z., Durmus Z., Caglar Y., Caglar M., Turut A., Electrical characterization of Ir doped rare-earth orthoferrite $YbFeO_3$, *Journal of Alloys and Compounds,* 787 (2019) 1212-1224.

[7] Coskun M., Polat O., Coskun F. M., Kurt B. Z., Durmus Z., Caglar M., Turut A., The Impact of Ir Doping on the Electrical Properties of $YbFe_{1-x}Ir_xO_3$ Perovskite-Oxide Compounds, *J. Mater. Sci.: Mater. Electron*., 31 (2020) 1731.

[8] Polat O., M. Coskun, Kalousek R., Zlamal J., Kurt B. Z., Caglar Y., Caglar M., Turut A., Frequency and Temperature-Dependent Electric Modulus Spectroscopy of Os Doped $YbFeO_{3-\delta}$ Structure, *J. Phys.: Condens. Matter.,* 32 (2020) 065701.

[9] Polat O., Caglar M., Coskun F. M., Coskun M., Caglar Y., Turut A., An investigation of the optical properties of $YbFe_{1-x}Ir_xO_{3-\delta}$ (x=0, 0.01 and 0.10) orthoferrite films, *Vacuum,* 173 (2020) 109124.

[10] Polat O., Caglar M., Coskun F. M., Coskun M., Caglar Y., Turut A., Examination of Optical Properties of $YbFeO_3$ films via Doping Transition Element Osmium, *Optical Materials,* 105 (2020) 109911.

[11] Polat O., Caglar M., Coskun F. M., Coskun M., Caglar Y., Turut A., An Experimental Investigation: The Impact of Cobalt Doping on Optical Properties of $YbFeO_{3-\delta}$ Thin Film, *Mater. Res. Bull*., 119 (2019) 110567.

[12] Polat O., Coskun M., Coskun F. M., Zlamal J., Kurt B. Z., Durmus Z., Caglar M., Turut A., Co doped $YbFeO_3$: exploring the electrical properties via tuning the doping level, *Ionics,* 25 (2019) 4013–4029.

[13] Liferovich R. P., Mitchell R. H., A structural study of ternary lanthanide orthoscandate perovskites, *J. Solid. State. Chem.,* 177 (2004) 2188.

[14] Magome E., Moriyoshi C., Kuroiwa Y., Masuno A., Inoue H., Noncentrosymmetric Structure of $LuFeO_3$ in Metastable State, *Japan. J. Appl. Phys*., 49 (2010) 09ME06.

[15] Leelashree S., Srinath S., Investigation of Structural, Ferroelectric, and Magnetic Properties of La-Doped $LuFeO_3$ Nanoparticles, *J. Supercond. Nov. Magn*., 33 (2020) 1587–1591.

[16] Wang W.B., Zhao J., Wang W.B., Gai Z., Balke N., Chi M.F., Lee H.N., Tian W., Zhu L., Cheng X.M., Keavney D.J., Yi J.Y., Ward T.Z., Snijders P.C., Christen H.M., Wu W.D., Shen J., Xu X.S., Room-temperature multiferroic hexagonal $LuFeO_3$ films, *Phys. Rev. Lett.,* 110 (2013) 237601.

[17] Coskun M., Synthesis, Characterization and Electrical Admittance Study of $LaCrO_3$ Perovskite Compound, *Int. J. Adv. Eng. Pure Sci*. 1 (2019) 29-35.

[18] Holinsworth B.S., Mazumdar D., Brooks C.M., Mundy J.A., Das H., Cherian J.G., McGill S.A., Fennie C.J., Schlom D.G., Musfeldt J.L., Direct band gaps in multiferroic h-$LuFeO_3$, *Appl. Phys. Lett.,* 106 (2015) 082902.

[19] Zhu L.P., Deng H.M., Sun L., Yang J., Yang P.X., Chu J.H., Optical properties of multiferroic $LuFeO_3$ ceramics, *Ceram. Int.,* 40 (2014) 1171-1175.

[20] Zhou M., Yang H., Xian T., Zhang C.R., A new photocatalyst of $LuFeO_3$ for the dye degradation, *Phys. Scripta,* 90 (2015) 085808.

[21] Suresh P., Laxmi K. V., Kumar P.S., Enhanced room temperature multiferroic characteristics in hexagonal $LuFe_{1-x}Ni_xO_3$ ($x = 0 - 0.3$) nanoparticles, *J. Magn. Magn. Mater.,* 448 (2018) 117-122.

[22] Sarkar T., Manna K., Elizabeth S., Anil Kumar P.S., Investigation of multiferroicity, spin-phonon coupling, and unusual magnetic ordering close to room temperature in $LuMn_{0.5}Fe_{0.5}O_3$, *J. Appl. Phys.,* 121 (2017) 084102.

[23] Lurgo F. E., Billoni O. V., Pomjakushin V., Bolletta J. P., Martin C., Maignan A., Carbonio R. E., Signs of superparamagnetic cluster formation in $LuFe_{1-x}Cr_xO_3$ perovskites evidenced by magnetization reversal and Monte Carlo simulations, *Phys. Rev. B,* 103 (2021) 014447.

[24] Lin L., Zhang H. M., Liu M. F., Shen S., Zhou S., Li D., Wang X.,. Yan Z. B, Zhang Z. D., Zhao J., Dong S., Liu J.M., Hexagonal phase stabilization and magnetic orders of multiferroic $Lu_{1-x}Sc_xFeO_3$, *Phys. Rev. B,* 93 (2016) 075146.

[25] Liu J., Sun T.L., Liu X.Q., Tian H., Gao T.T., Chen X.M., A novel room-temperature multiferroic system of hexagonal $Lu_{1-x}In_xFeO_3$, *Adv. Funct. Mater.,* 28 (2018) 1706062.

[26] Leelashree S., Srinath S., Investigation of structural, ferroelectric, and magnetic properties of La-doped $LuFeO_3$ nanoparticles, *J. Supercond. Nov. Magnetism*, 33 (2019) 1587-1591.

[27] Polat O., Altering magnetic and optical features of rare earth orthoferrite $LuFeO_3$ ceramics via substitution of Ir into Fe sites, *Journal of Solid State Chemistry,* 305 (2022) 122701.

[28] Polat O., Coskun M., Roupcová P., Sobala D., Durmus Z., Caglar M., Sikola T., Turut A., Influence of iridium (Ir) doping on the structural, electrical, and dielectric properties of LuFeO3 perovskite compound, *Journal of Alloys and Compounds,* 877 (2021)160282.

[29] Pattanayak S., Parida B.N., Das P. R., Choudhary R.N.P., Impedance spectroscopy of Gd-doped $BiFeO_3$ multiferroics. *Appl. Phys. A,* 112 (2013) 387

[30] Jonscher A. K., The 'universal' dielectric response, *Nature,* 267 (1977) 673.

[31] Petrovsky V., Manohar A., Dogan F., Dielectric constant of particles determined by impedance spectroscopy*, J. Appl. Phys.*, 100 (2006) 014102

[32] Cheng P. F., Song J., Wang Q. P., Li S. T., Li J.Y., Wu K.N., Fine representation of dielectric properties by impedance spectroscopy, *Journal of Alloys and Compounds,* 740 (2018) 36-41.

[33] Sekrafi H. E., Kharrata A. B. J., Wederni M.A., Khirouni K., Boudjadaa N. C., Boujelben W., Structural, electrical, dielectric properties and conduction mechanism of solgel prepared $Pr_{0.75}Bi_{0.05}Sr_{0.1}Ba_{0.1}Mn_{0.98}Ti_{0.02}O_3$ compound, *Mater. Res. Bull*., 111 (2019) 329–337.

[34] James A. R, Srinivas K., Low temperature fabrication and impedance spectroscopy of PMN-PT ceramics, *Mater. Res. Bull*., 34 (1999) 1301.

[35] Sinclair D.C., West A.R, Impedance and modulus spectroscopy of semiconducting BaTiO3 showing positive temperature coefficient of resistance, *J. Appl. Phys.,* 66 (1989) 3850.

[36] Auwal I.A., Erdemi H., Sözeri H., Güngüneş H., Baykal A., Magnetic and dielectric properties of Bi^{3+} substituted $SrFe_{12}O_{19}$ hexaferrite, *J. Magn. Magn. Mater.,* 412 (2016) 69-82.

[37] Keelani A. O. A., Husain S., Khan W., Temperature dependent dielectric properties and ac conductivity of $GdFe_{1-x}Mn_xO_3$ ($0 \le x \le 0.3$) perovskites, *J. Mater. Sci.: Mater. Electron.,* 30 (2019) 20119–20131.

[38] Polat O., Coskun M., Roupcová P., Sobala D., Durmus Z., Caglar M., Sikola T., Turut A., The Os substitution into Fe sites in $LuFeO_3$ multiferroic and its effects on the electrical and dielectric properties, *Journal of Alloys and Compounds* 911, (2022) 165035.